

# Optimal Spar Design

Sailplane's Horizontal Stabilizer Spar  
Design Report

AE1222-I Group E02G

Delft University of Technology

# Optimal Spar Design

## Sailplane's Horizontal Stabilizer Spar Design Report

by

**AE1222-I Group E02G**

Lukas Moser (5902673)

Luuk van Breugel (6006183)

Bartosz Regulski (5907950)

Frederique Gransbergen (6004342)

Lucas Wilms (5922682)

Claudia van Daatselaar (5968674)

Aliz Atina Varró (5953901)

Pradyumn Mishra (5934559)

Samuël Zwaan (5997496)

Mario Larrondo (5903939)

Dimitar Sotirov (5917743)

Instructor: L. Compagne

Project Duration: April 2024 - June 2024

Faculty: Faculty of Aerospace Engineering, Delft

Cover image: Samuël Zwaan, Personal collection



# Summary

DELTA is designing a new sailplane that requires a wing spar for the horizontal stabiliser. The spar must withstand the loads during all phases of flight while performing its aerodynamic load. DELTA sets out 2 key requirements for the wing spar. First, it needs to sustain a load of 1.1 kN discretely distributed via a whiffletree without failure, and second, the final mass of the spar needs to be less than 2552 g. There is also a heavy emphasis on designing a sustainably manufactured spar. Additionally, DELTA has constrained the overall dimensions and the material the spar is to be made of.

This report aims to propose, test, and analyse a wing-spar configuration for DELTA's new sailplane. The design is based on a literature study, and the design phase including calculations, manufacturing, and testing.

The process started with a literature study, to dive into the subject of wings and spars, and find the answer to preliminary questions. Second, a configuration that supports the load was decided upon. After this decision, the spar's mass was incrementally reduced until the requirement was also met. The first design to successfully meet these criteria was then manufactured and subsequently tested. The testing is carried out by a whiffletree, and the deflection was measured, while the spar was visually observed. The report ends with a conclusion followed by recommendations.

The final design of the spar weighs 2551 g and consists of a full-size X-sheet at the root and a 750 mm cut at the tip, two 750 mm Y-sheets at the root and two full-sized ones at the tip, forming the flanges. Also, 21 holes, eight 1125 mm stringers, connect the web to the two flanges and 34 bolts and nuts. The final design can be seen in Figure 1.

The results of the testing showed the spar had performed adequately, but it started to buckle significantly before the target load requirement. This occurred due to the lack of bolts close to the root of the wing spar. The top sheet ended up buckling at around 1 kN and experienced a total load of 1.2 kN during testing. But, testing has not gone as far as failure.

All in all, the spar meets the requirements set and should be a good solution for the new sailplane. It is recommended to reiterate the process, ensuring there are more bolts towards the root, while more holes are made to accommodate for the added mass. This strengthens the spar where it failed first during testing and is thus perfect for iteration.

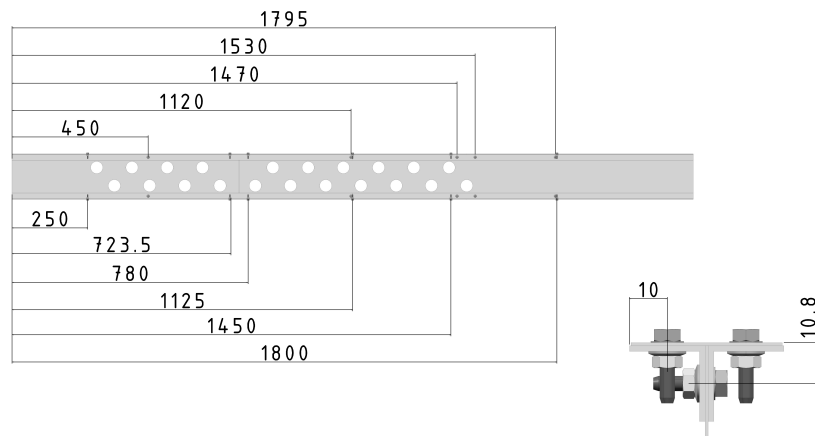


Figure 1: Final design

# Contents

<b>Summary</b>	<b>i</b>
<b>List of Symbols</b>	<b>iv</b>
<b>List of Figures</b>	<b>v</b>
<b>List of Tables</b>	<b>vi</b>
<b>1 Introduction</b>	<b>1</b>
<b>2 Study of Wing Spars and Their Manufacturing</b>	<b>2</b>
2.1 Function of a Spar . . . . .	2
2.2 Differences between Wing Spar and Wing Box . . . . .	2
2.3 Life cycle of a Wing Spar and an Aircraft . . . . .	3
2.4 Operating Conditions for a Sailplane . . . . .	3
2.5 Safety Factor . . . . .	4
2.6 Loads at Various Phases of Flight . . . . .	4
2.7 Dynamic Loads . . . . .	6
2.8 Structural Failure . . . . .	7
2.9 Comparison of Robot Production and Manual Labor . . . . .	7
2.10 Comparison of Bolted and Riveted Structures . . . . .	7
<b>3 Design of Wing Spar</b>	<b>9</b>
3.1 Design Requirements . . . . .	9
3.2 Assumptions and Simplifications . . . . .	11
3.3 Iterative Design Process . . . . .	12
3.3.1 Moment of Inertia . . . . .	12
3.3.2 Shear Buckling . . . . .	13
3.3.3 Explanation and Justification of Design Choices . . . . .	14
3.4 Final Design . . . . .	16
<b>4 Manufacturing of Wing Spar</b>	<b>18</b>
4.1 Description of the Manual Production Plan . . . . .	18
4.2 Assessment of the Predicted vs. Actual Person-hours during Manual Manufacturing . . . . .	18
4.3 Analysis of Nonconformities and Their Influence . . . . .	19
4.4 Description of the Robotic Production Plan . . . . .	20
4.5 Assessment between Manual and Robotic Manufacturing . . . . .	20
4.6 Recommendations for Manufacturing . . . . .	20
<b>5 Sustainability</b>	<b>22</b>
5.1 Economic Model . . . . .	22
5.2 Manufacturing Waste . . . . .	22

5.3 Recyclable Aircraft . . . . .	22
5.4 Explanation and Justification of Design Choices with respect to sustainability . . . . .	23
5.5 Assessment of Spar's Lifetime Cycle . . . . .	23
5.6 Explanation and Justification of Manual vs. Robotic Manufacturing . . . . .	24
<b>6 Testing and Analysis</b>	<b>25</b>
6.1 Test Objective and Setup . . . . .	25
6.2 Calculation of load distribution . . . . .	26
6.3 Utilized Testing Instrumentation . . . . .	27
6.4 Test Plan . . . . .	28
6.5 Test Events . . . . .	29
6.6 Failure area analysis . . . . .	30
6.7 Comparison with predictions . . . . .	31
6.8 Possible Improvements . . . . .	31
<b>7 Conclusion</b>	<b>32</b>
<b>Bibliography</b>	<b>33</b>
<b>A Plots of Test Data and Events</b>	<b>36</b>
<b>B Calculations Done for Beam Hole Placements</b>	<b>38</b>
<b>C Statement on AI Usage</b>	<b>39</b>
<b>D Gantt Chart</b>	<b>40</b>
<b>E Task Distribution</b>	<b>41</b>

# List of Symbols

$\delta$	Deflection	mm
$\rho$	Density	$\text{kgm}^{-3}$
$\rho_m$	Material Density	$\text{gcm}^{-3}$
$\sigma_{ult}$	Ultimate Stress	MPa
$\sigma_y$	Yield Stress	MPa
$\tau_{cr}$	Critical Shear Buckling	MPa
$\theta$	Angle of Twist	rad
$A$	Area	$\text{m}^2$
$d$	Distance to Neutral Axis	m
$E$	Young's modulus	MPa
$F$	Force	N
$h$	Height	m
$I$	Moment of inertia	$\text{m}^4$
$K_s$	Buckling coefficient	-
$L$	Length	m
$M$	Moment	Nm
$m$	Mass	g
$p$	Pressure	Pa
$q$	Distributed Force	$\text{Nm}^{-1}$
$q$	Shear flow	$\text{Nm}^{-1}$
$R$	Reaction Force	N
$T$	Temperature	K
$T$	Torque	Nm
$t$	Thickness	m
$v$	Velocity	$\text{ms}^{-1}$
$W, b$	Width	m

# List of Figures

1	Final design . . . . .	i
2.1	Different loads on the horizontal stabilizer during taxi, takeoff, cruise, and landing. . . . .	5
2.2	Wing deflection due to inertial loads [1] . . . . .	5
2.3	Wing deflection due to aerodynamic and gravitational loads [2] . . . . .	5
2.4	The two types of deflection that occur during cruise, landing, and takeoff. . . . .	6
2.5	The whiffle tree setup on a wind turbine blade. . . . .	6
2.6	Bending of the wing due to wind forces . . . . .	7
3.1	Wing spar concept proposed by DELTA: an I-beam design . . . . .	10
3.2	Schematic showing wing spar clamp setup (cross-section) . . . . .	10
3.3	Internal shear and moment diagram of the whiffletree setup. . . . .	11
3.4	I-beam cross-section . . . . .	13
3.5	Shear buckling coefficients for skin-stiffener panel [3] . . . . .	14
3.6	A shear-location graph comparing critical shear in a continuous sheet (navy blue), critical shear in the presence of a 40mm hole (orange), and the experienced shear stress (blue) . . . . .	15
3.7	Positioning of the bolts . . . . .	16
3.8	Positioning of the holes . . . . .	16
6.1	Side view of whiffletree setup with the load application at Point S. . . . .	25
6.2	Clamp system for whiffletree connection points. . . . .	26
6.3	Free body diagram of the beam. . . . .	26
6.4	Sensors . . . . .	27
6.5	Sensor box test and calibration setup: note the load cell with a rod to add different weights. . . . .	28
6.6	Buckling at the web plate and top sheet close to the clamp . . . . .	29
6.7	Plot of the force against displacement during testing. Force vs time and displacement vs time plots are displayed in Appendix A along with the code that generated them. . . . .	30
A.1	Plots of the collected test data in load vs displacement, load vs time and displacement vs time. . . . .	36

# List of Tables

3.1	Material availability list . . . . .	10
3.2	Alu-maximum material properties . . . . .	10
3.3	Factory nuts and bolts specifications . . . . .	10
3.4	Moment of inertia . . . . .	13
3.5	Buckling Shear Calculations for example values . . . . .	14
3.6	Mass calculation of the final beam. . . . .	15
4.1	Comparison of predicted to actual work time per stage . . . . .	19
4.2	Comparison between the cost of robotic and manual manufacturing . . . . .	21
5.1	Comparison of manual and robotic manufacturing energy consumption . . . . .	24
C.1	AI tools Used . . . . .	39



# 1

## Introduction

In a world in which the topics of global warming and the greenhouse effect gain importance every day, the demand for sustainable solutions continues to rise. The company DELTA, a leader in aircraft manufacturing, is committed to reducing the environmental impact of its products. They asked the Important Aerospace Company (IAC) to design the wing structure for their new sailplane, which must become a sustainable and 100%-recyclable aircraft.

Project Feather Wing involves designing a sailplane for two passengers, capable of flying at 300 knots. It will have a wing span of 19 meters and a maximum take-off weight of 750 kg. All the expected loads that the sailplane will encounter throughout its lifetime were determined and translated into a prescribed load that the spar of the horizontal stabilizer must endure.

The aim of this report is to propose, test and analyse a wing-spar configuration to be used in the tail of the aircraft in Project Feather Wing. IAC has already provided a certain set of components to use and also specified the size of the spar and its maximum mass. The process consists of first researching the general requirements that a wing spar needs to fulfil. Afterwards, the ideal configuration will be determined by designing a spar that can sufficiently carry the required loads and then minimising the mass without affecting the structural integrity. The manufactured wing-spar will then be tested and the outcome will be analysed.

In addition to the design, DELTA wants the IAC to write a production plan for the wing spar that can be executed in the IAC aeroplane hall. DELTA is also exploring the feasibility of shifting wing production from manual labour to automatic manufacturing, which requires that segments of the wing production process be automated and that those parts have to be programmed for a robot. Finally, the wing spar will be tested using a whiffletree.

This report is structured as follows; before starting the design, the team conducted a literature study of wing spars and their manufacturing. The findings of which are described in Chapter 2. In Chapter 3, the design process of the wing spar is explained. The manufacturing and testing of the wing spar are described in Chapter 4 and Chapter 6, while Chapter 5 dives into the details of the sustainability aspects of this design.

Through Project Feather Wing, DELTA aims to take new steps in sustainable aviation, using new technologies and trying to achieve 100% sustainability. These innovative ideas address the growing issue of climate change and demonstrate to the world that there are also less polluting solutions.

# 2

## Study of Wing Spars and Their Manufacturing

In this section, key aspects of wing spars and their manufacturing processes are investigated to provide context before starting the design process. It is necessary to thoroughly understand the context around a wing spar, otherwise, the proposed design may be lacking in several aspects or may be impractical to construct.

### 2.1. Function of a Spar

The primary function of a spar is to transmit the loads experienced by the wings to the main body of the aircraft, the most important of which is the bending moment due to the lift [4]. Other loads include both compressive and tensile forces from the spar caps, but also a torsional load. Without a reinforcing spar, the wings would deform, possibly leading to the failure of the aircraft as a whole [4].

Spars also serve as the framework of the wing, often referred to as its 'skeleton.' They support the ribs, which give the wings their shape, and aid in torsional load relief [4].

### 2.2. Differences between Wing Spar and Wing Box

Having a short description of the commonalities and differences between the wing box structure and the wing spar at hand aids in understanding the usefulness of each in given situations.

- The Wing Box is a component of an aircraft's wing and is called that way due to its box-like shape when looking at the cross-section of the wing.
- The Wing Spar is a beam that runs horizontally through the wing from the fuselage to the tip of the wing, acting as a backbone.

These systems are two common approaches to handle, bundle, and transfer wing loads from the wing into the fuselage (or in this case, into the vertical stabilizer since the tail configuration is a T-shape). While a wing box consists of multiple parts, most often spars in the front and back and skin panels on the top and bottom (sometimes reinforced [5]), the wing spar only consists of one part, namely the spar itself.

Comparing them with each other, roughly results in flexibility versus mass-to-strength ratio trade-off [6]. The wing box is more versatile due to its shape and can act as a platform that allows for mounting non-structural components such as fuel tanks or control surfaces [6]. When optimizing performance, a single wing spar can be shaped to the given application while a box is fixed with its rectangular shape [6]. If optimising for minimal deflection, for example, the I-profile is more beneficial than a box beam [6].

Also manufacturing is simplified with a wing spar due to the reduced part count and especially for smaller aircraft, assembly, and integration can be more time and labour-intensive as it requires more precision for box-shaped load-bearing structures than for a simple I-shaped spar [7].

## 2.3. Life cycle of a Wing Spar and an Aircraft

The start of the life cycle of a wing spar is the extraction of the materials used to produce a wing spar. Wing spars are typically made out of aluminium [8]. Extracting aluminium still has quite a large carbon footprint, improvements in that area are being worked on [9].

After the material extraction comes the manufacturing and processing of the wing spar. Wing spars are made using manufacturing methods like riveting, welding, casting forging, extrusion, and machining of an aluminium plate [10][11]. Welded or riveted wing spars are the normal configuration. These methods will have a carbon footprint from the machinery and materials used.

The next phase of the life cycle is the transportation of the wing spar and the aircraft. The environmental impact of transporting the wing spar heavily depends on the location of the manufacturing process relative to the final assembly's location. The carbon footprint of transportation can be relatively high because the parts that have to be transported can be quite big and sometimes need to travel far. Often parts are transported by another plane, and the carbon emissions of aircraft are high.

Once the aircraft gets to the customer, the life cycle phase of the usage of the aircraft starts. Aircraft are used in many different fields, such as the commercial sector, the military sector, the transportation sector, and the private sector. These all use different types of aircraft with different carbon footprints. The emissions during flight, as well as the emissions from all the ground operations. As of now, aircraft contribute to 2% of the world's carbon emissions, so the carbon footprint of an aircraft operating life is high [12]. This report however focuses on a sailplane, which does not use an engine, so the carbon footprint of its usage will be low compared to other aircraft.

Once an aircraft goes out of service, it needs to be disposed of. An aircraft can be disassembled and its materials can be recycled if they are retrieved the right way [13]. This would improve the sustainability of an aircraft since its components will be recycled. The process does still contribute to emissions of the aircraft life cycle, but then the emissions from the material extraction phase can be reduced. A wing spar will not be made out of too many different materials, so the recycling of this part is very much possible[14].

## 2.4. Operating Conditions for a Sailplane

A sailplane operates without using an engine. Launching a sailplane is generally done with a winch or an aero tow. After launch, it uses thermals to keep flying. Thermals are currents of rising air caused by uneven heating of the earth. A sailplane can also be kept in the air with ridge lift and wave lift. Ridge lifts are currents of air going upwards because of deflecting against a hill, while wave lifts are caused by air that bounces off the ground, going back up [15].

Sailplanes are allowed to fly at an altitude of up to 19500 ft (5944 m), but will generally go up to 15000 ft (4572 m) high [15]. This means sailplanes stay in the troposphere during their flight. At an altitude of 4.6 km, the temperature is 259 K, the pressure is 57750 Pa, and the density is  $0.6343 \text{ kg/m}^3$ . A sailplane normally reaches a speed of about 20-30 m/s [16]. These values provide information on what conditions the sailplane that will be designed needs to be able to withstand.

## 2.5. Safety Factor

To ensure the safety of a structural or mechanical member, it is necessary to restrict the applied load to one that is less than the load the member can fully support. Safety factors are applied to provide a safety reserve between expected conditions and actual conditions that could cause failure or damage [17]. Clausen and Hansson define five main categories of uncertainties in structural engineering: higher loads than expected, the material performing worse than expected, imperfect theory of the failure mechanism in question, potential unknown failure mechanisms, and human error in design or manufacturing [18]. According to Hibbeler [19], Modlin and Zipay [20], the following reasons are relevant to this

- Inadvertent In-Service Loads greater than the design limit.
- Inexact measurements of a structure or machine, due to fabrication or assembly errors.
- Structural deflections above limit load that could compromise vehicle structural integrity.
- Several materials, such as wood, concrete, or fibre-reinforced composites, demonstrate high variability in mechanical properties, thus one cannot be sure about the exact properties of the final product.

The safety factor is defined as the ultimate load divided by the allowable load, or alternatively, the design overload divided by the normal load [21].

According to Modlin and Zipay a 1.5 safety factor is established for the design of aircraft - it is observed that aeroplanes currently flying that were designed with a sufficient safety factor fly very safely. A higher safety factor would require a heavier structure, which is not economical for an aircraft. Modlin and Zipay also note that high safety factors do not guarantee no failures - a high safety factor cannot overcome inadequate design practice, ineffective quality control, incorrect structural analysis, or brittle material failures.

The safety margin has a similar purpose but differs from it by definition. It is the safety factor minus one and is the range between the most adverse condition accounted for and the worst-case scenario that could happen [21]. A relevant difference is that the safety factor is multiplicative and the safety margin is additive [18].

## 2.6. Loads at Various Phases of Flight

During flight, a horizontal stabilizer will be subjected to different loads in various phases of flight, such as taxi, takeoff, cruise, and landing.

- While taxiing, no significant aerodynamic loads are exerted on the stabilizer. The main component is the gravitational load of the horizontal stabilizer itself and inertial loads during e.g. acceleration.
- In the takeoff phase, inertial loads during the high acceleration act on the horizontal stabilizer. Aerodynamic loads are introduced as the speed of air over the airfoil increases. In addition, during takeoff, the horizontal stabilizer adjusts and maintains the aircraft's pitch attitude using the elevators. This adds to the stabilizer's loads.
- In cruise, the horizontal stabilizer uses trim to keep the aircraft stable. Thus, the only loads acting on the stabilizer are aerodynamic loads. Also, its own gravitational load which in flight serves as a relief moment, actually decreases the total (upward) forces.

- The landing phase is similar to the takeoff phase. The deceleration of the aircraft produces inertial loads. Aerodynamic loads and the horizontal stabilizer adjusting the aircraft's pitch attitude using the elevators add to the different loads acting on the stabilizer.

In Figure 2.1, the free-body diagrams have been added to indicate the loads during the various phases of flight.

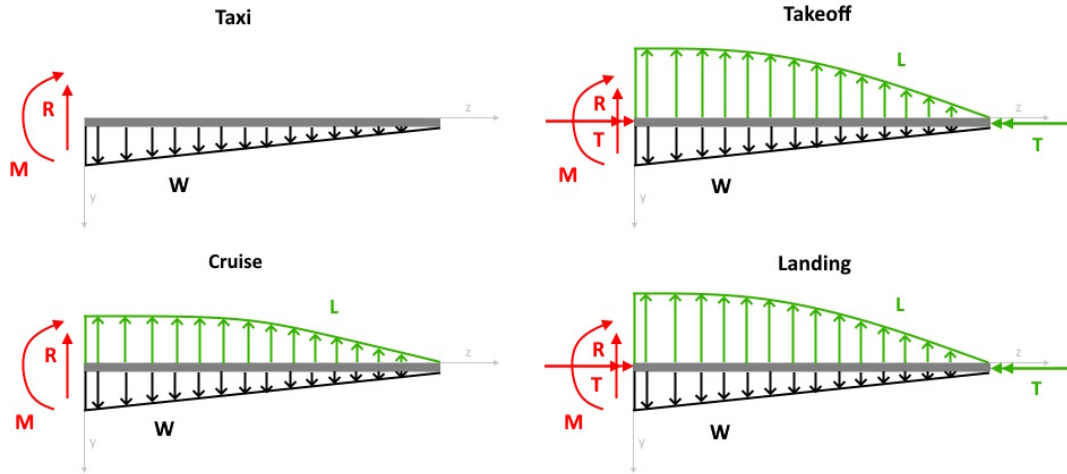


**Figure 2.1:** Different loads on the horizontal stabilizer during taxi, takeoff, cruise, and landing.

Due to the different loads acting on the horizontal stabilizer, it deflects. This is due to Wing-Root Bending Moments, Wing-Root Torsional Loads, Wing-Tip Torsional Loads and Flutter Susceptibility [22]. This deflection can have various forms like those presented in 2.3 and 2.2.

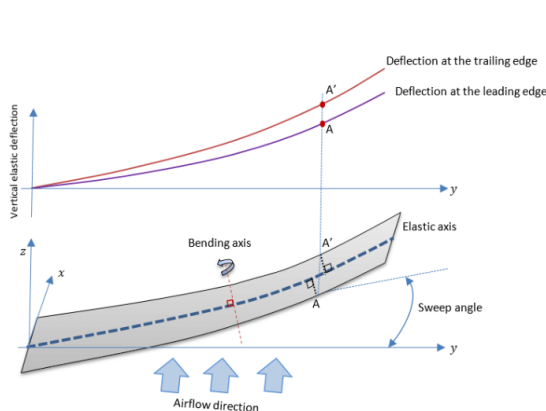


**Figure 2.2:** Wing deflection due to inertial loads [1]

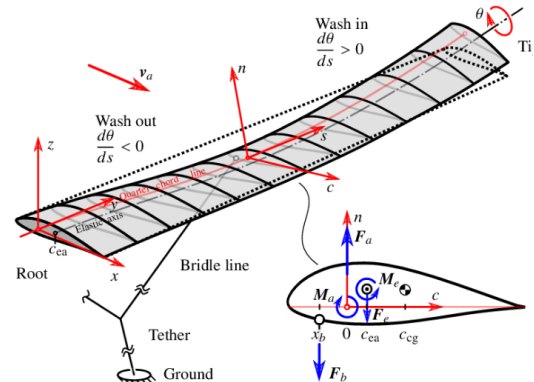


**Figure 2.3:** Wing deflection due to aerodynamic and gravitational loads [2]

In Figure 2.5 the horizontal stabilizer for the different phases of flight has been sketched. The second deflection during cruise is negligible.

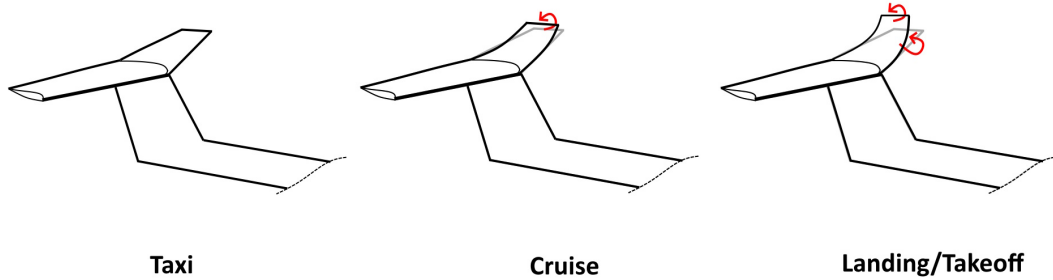


**Figure 2.4:** The two types of deflection that occur during cruise, landing, and takeoff.

### Load Simulation

When testing the wing spar, it is preferred to simulate the real-life loads as best as possible. The loads in the real aircraft are mainly distributed loads over the entire wing surface, as a function of the chord in that section. As the wing tapers the load will decrease with the span of the wing. This distributed load can be simulated in a whiffletree setup. In this setup the load is distributed using several cables and spreader bars [23]. This setup can mimic the loads of cruise flight, landing, and take-off if configured correctly. To achieve the most accurate distributed load the number, length, and position of spreader bars can be adjusted.

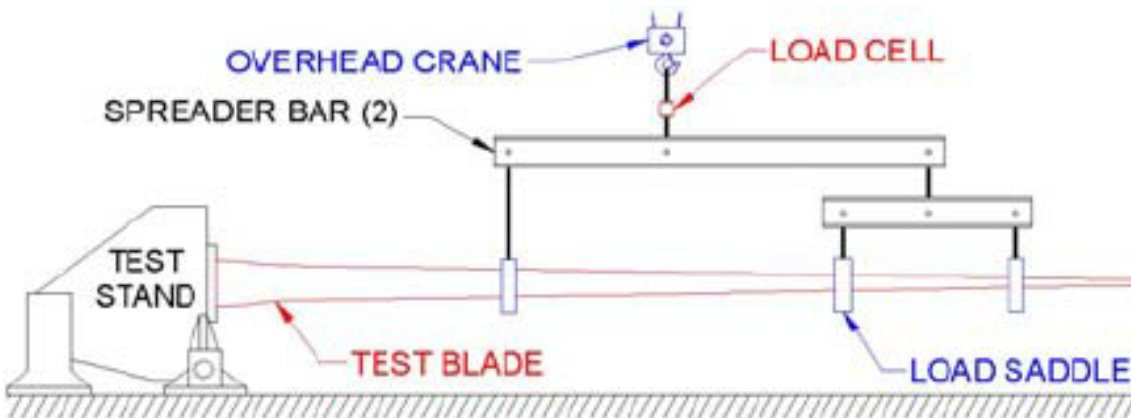


**Figure 2.5:** The whiffle tree setup on a wind turbine blade.

## 2.7. Dynamic Loads

Besides static loads, there are also dynamic loads acting on a horizontal stabilizer. A dynamic load is a load that is constantly changing over time [24]. An example of a dynamic load is a person that is jumping on the ground. The person exerts an unstable force on the ground which changes over time.

Aerodynamic loads can cause deformation of the structure. The wings will bend due to the wind forces which prevents them from failure. The horizontal stabilizer of the aircraft must take care of the stability of the aircraft and therefore it must not bend. In Figure 2.6 one can see that the stabilizer needs to stay straight to retain stability [25].

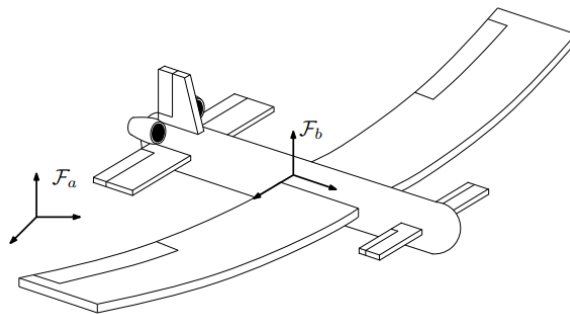


**Figure 2.6:** Bending of the wing due to wind forces

The influence of wind forces on the design of the horizontal stabilizer is that the spar has to be made of a stiff material to prevent bending and failure.

Another instance of dynamic loading can be when the horizontal stabilizer impacts something. When this happens the spar should withstand this impact. This impact can be anything from hitting an aircraft hanger door to a bird strike midflight.

Pressure fluctuations also create aerodynamic loads. When an airplane flies faster a higher pressure is applied to the bottom of the horizontal stabilizer. This pressure creates a higher lift to the stabilizer. When the pressure changes quickly the lift changes as well. When designing the horizontal stabilizer the area can be increased to increase the lift the horizontal stabilizer can obtain [26].

## 2.8. Structural Failure

Structural failure is defined as the loss of load-carrying capacity. It can happen due to various reasons, including design errors, micro-structural defects, loading conditions, human errors, and environmental exposure and their combinations. The most common sources of sudden structural failure are corrosion and fatigue, accounting for 90% of failures in metallic alloys. Premature failure can be accelerated at locations where stress is concentrated, for example, notches, holes, or tight fillet radii [27].

## 2.9. Comparison of Robot Production and Manual Labor

In this day and age, technology advancements allow industries to incorporate increasing amounts of robots on their production lines [28]. What might be the advantages and disadvantages of production performed by robots compared to manual labour? A survey on human-robot collaboration in industrial settings performed by Valeria Villani [29] points out that robots prefer tasks with "high levels of accuracy, speed and repeatability". Furthermore, after the initial implementation of a robot, its' labour is cheaper compared to a human. It is emphasized by Golda, Kampa, and Paprocka [30] that "Since human factors affect the production processes stability, robots are preferred to apply. The application of robots is characterized by higher performance and reliability compared to human labour". Apart from these financial aspects, production robots have more strength and precision. Robots can be used as enhancements for tasks that humans are mediocre at. Nevertheless, it has to be kept in mind that robots still require humans to oversee them and solve problems when they arise.

## 2.10. Comparison of Bolted and Riveted Structures

During the manufacturing process of metal structures, there are different methods for joining different elements together. The two most used techniques are bolting and riveting, which offer dif-

ferent properties in the structural, maintenance, and production perspectives. Analysis conducted both analytically and experimentally concluded that riveting provides more endurance for various pitch dimensions compared to bolting [31]. However, a study carried out in the field of helicopter airframes [32] suggests that rivet joints experience more fatigue than bolted joints, increasing maintenance costs. Furthermore, bolted connections can be installed with standard handheld tools and can be reused, while rivets require specialized tooling and their installation is generally more time-consuming.

# 3

## Design of Wing Spar

This section goes through the design process for the wing spar while explaining and justifying decisions. The aim is to design a spar that can sustain the required loads but also keep the total mass below a certain value.

### 3.1. Design Requirements

A Design Requirement List is a list of statements that quantifiable provides on what a system is obliged to do and how well and under what constraints. For the design of the wing spar, DELTA has set the following requirements:

- Failure shall occur at an applied load of 1.1 kN or greater, measured on point S of the whiffle-tree test setup as can be seen in figure 6.1.
- The total mass of the assembled beam shall be less than 2552 grams.
- The structure has to be optimized for sustainable manufacturing, operations, and end-of-life considerations.

In addition, Delta has given the following design constraints:

- The spar is an I-beam structure, giving overall dimensions of 2250 x 150 x 41mm, see Figure 3.1
- Table 3.1 and Table 3.2 provide an overview of the materials available to the team and their properties
- All sheet metal shall be connected using bolts. Bolt specifications are given in Table 3.3
- In the first 150mm of the spar, there shall be no bolts, due to clamping constraints from the test jig (see Figure 3.2)
- The last 250mm of the spar web shall be of continuous skin (no interruptions), to accommodate the elevator connection bracket

In addition, the IAC wants to incorporate principles of a new economic model that is conducive to accomplishing environmental goals. DELTA is committed to reducing the environmental impact of its products over their lifetime. Thus, sustainability must be actively considered in the wing design.

**Table 3.1:** Material availability list

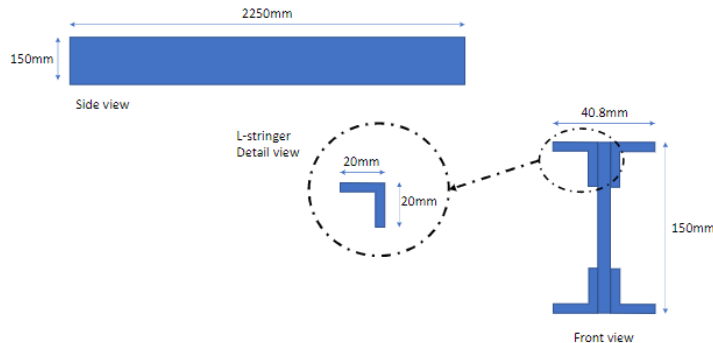
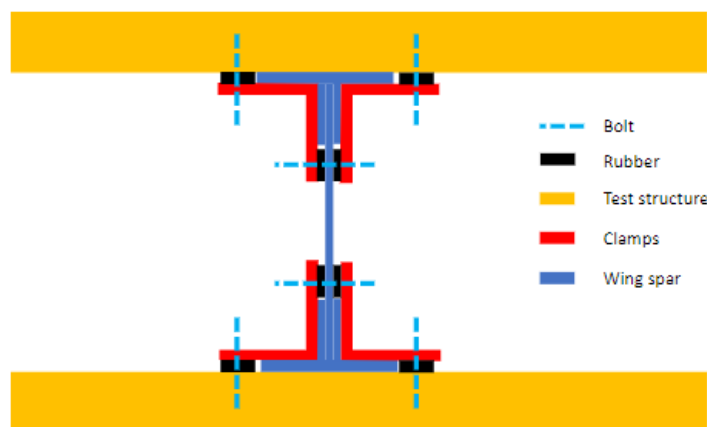
Item	Quantity	L [mm]	W [mm]	t [mm]	Notes
Sheet X	3	1500	148.4	0.8	Web sheet (483 grams)
Sheet Y	4	1500	40.0	0.8	Top/bottom sheet (128 grams)
L-Stringer Z	8	1500	20x20	1.5	Stringer (237 grams)
Bolts	60	-	-	-	Bolt weight 1.39 gram
Nuts	60	-	-	-	Nut weight 0.94 gram

**Table 3.2:** Alu-maximum material properties

$\sigma_{ult}$ [MPa]	$\sigma_y$ [MPa]	E [MPa]	$\rho_m$ [g/cm <sup>3</sup> ]
483	345	71700	2.78

**Table 3.3:** Factory nuts and bolts specifications

Article description	Article number
Hexagon nut A2 M4	51112040010
Flange bolt DIN 7500 D M4X16	27000040016

**Figure 3.1:** Wing spar concept proposed by DELTA: an I-beam design**Figure 3.2:** Schematic showing wing spar clamp setup (cross-section)

## 3.2. Assumptions and Simplifications

Since economic and time-dependent limitations play a driving role in product design, assumptions have to be made to simplify the conditions of reality. These are carefully evaluated and listed in this section to keep track of the boundaries that these suppositions bring with them.

First, the final spar is assumed to act as a single entity that fails rather than sub-parts that are bonded together. This eases the calculation processes to not need to consider the bolts and sheets under separate loading. However, this requires that the bolts will not be the point of failure, so the maximum load a bolt experiences needs to be less than the maximum shear stress it can experience.

Second, the spar is assumed to not have any imperfections in the bolts or any of the sheets/stringers. The result of this is that the calculated load of failure will be higher than the actual load of failure as there is a degree of imperfection in any product. While this does make the process of designing easier, the possibility of failing to meet the criteria needs to be accounted for, the best way to do so is to incorporate a safety factor that can account for a certain degree of imperfection, beyond which it would not be reasonable to accept that the initial products were without fault.

Third, any combined loading will not be considered in the calculations. In Section 6.2, calculations of the loading of the whiffletree setup result in an internal force diagram (Figure 3.3). The main loading factor in this diagram is bending. In real life, there might be other loading going on simultaneously, like turbulence causing the spar to twist. This torsion load can impact the geometry of the spar and therefore negatively impact the performance of the spar in bending. This can be accounted for by a safety factor.

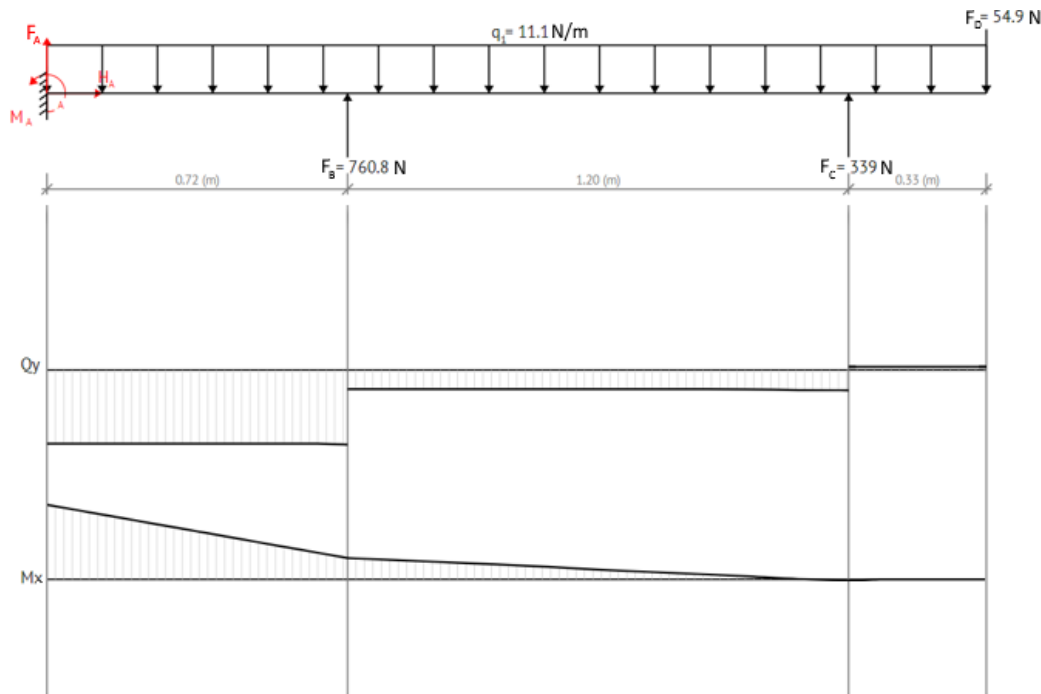


**Figure 3.3:** Internal shear and moment diagram of the whiffletree setup.

Fourth, the spar will have a constant cross-section. In practice, spars in wings tend to taper towards the wingtips due to the reduced required strength [33]. Deciding the point at which a sheet should not continue further is not an easy task and introduces a lot of variables. This decision will, however, yield a heavier spar than necessary as the whole length will be able to sustain the greatest loads which are only found at the root of the stabiliser.

Another simplification has been made considering the moment of inertia of the cross-section. The holes that will be made in the spar will influence the moment of inertia of the cross-section. This change should however be minimal, so to simplify the calculations for the moment of inertia, this change will be ignored yielding a larger moment of inertia than in reality.

Last, the failure calculations of the spar are done with the assumption that the holes for the bolts have no impact on the strength of the spar. The sheets/stringers are assumed to transfer loads evenly and continuously. In reality, the stress concentration at the holes is larger than at the other parts, but taking this into account for all the holes would make calculations significantly more complex. To avoid failure at a stress lower than calculated this is accounted for in the safety factor.

### 3.3. Iterative Design Process

After a preliminary idea is conceived, several iterations will refine the design. The goal is to minimise weight while still following the load-bearing requirements.

The initial design that was thought of had the web have a discontinuity towards the root of the stabiliser, 500mm in, but upon further consideration, the discontinuity was moved towards the tip, such that it is 500mm from the outer edge. This was decided since the loads become larger, the closer gets to the root so discontinuities are to be pushed as far out as possible.

A similar approach applies to the flanges. However, this means the stringers cannot have a discontinuity at the same place, otherwise the spar falls apart.

To meet the criteria of mass, lightening holes need to be made. The number of holes was determined by the maximal number the web could account for without losing significant shear strength. As a result, the remaining weight available was utilised for bolts to secure the individual components as well as possible. A balance needed to be reached as reducing the mass of the spar also reduces its strength and could lead to failure due to increased stress concentration.

#### 3.3.1. Moment of Inertia

To calculate the spar's failure load, first, the moment of inertia of the spar has to be calculated. The I-beam is symmetric and thus the moment of inertia of one side can be calculated and be multiplied by two.

The I-beam has been divided into several segments as can be seen in figure 3.4. For each of these segments, the moment of inertia is calculated using the formula 3.1. In this formula  $b$  is the width in meters,  $h$  is the height in meters,  $A$  is the area in meters squared, and  $d$  is the distance to the neutral axis in meters.

$$I_x = \frac{bh^3}{12} + Ad^2 \quad (3.1)$$

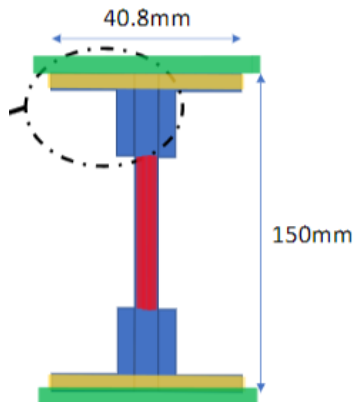


**Figure 3.4:** I-beam cross-section

In table 3.4 the calculated moment of inertia of all the segments and the total moment of inertia of the cross-section of the I-beam is stated.

**Table 3.4:** Moment of inertia

Segment	Moment of inertia [ $m^4$ ]
Green	$1.78087 * 10^{-7}$
Yellow	$3.30629 * 10^{-7}$
Blue	$2.92208 * 10^{-7}$
Red	$8.87333 * 10^{-8}$
Total	$1.69058 * 10^{-6}$

The total area moment of inertia sums up to  $1.69058 * 10^{-6} m^4$ . There are small differences in the moment of inertia throughout the beam because there are several lightening holes in the beam. Those holes will be made in the red segment of the cross-section, visible in Figure 3.4, but this segment has the smallest moment of inertia of the entire beam, and thus the alterations of the moment of inertia can be neglected as described in section 3.2. In the following calculations, it is assumed that the moment of inertia is constant throughout the entire beam.

### 3.3.2. Shear Buckling

A different failure condition that also needs to be accounted for is Shear Buckling. Knowing the maximum shear load is equal to 1020 N, calculated in Section 6.2, this value can be compared with the value obtained from Equation 3.2 [3]

$$\tau_{cr} = K_s E \left( \frac{t}{b} \right)^2 \quad (3.2)$$

, where  $K_s$  is the shear buckling coefficient,  $E$  is Young's Modulus,  $t$  is the plate thickness, and  $b$  is the plate width.  $K_s$  can be obtained from Figure 3.5. If the total 2250 mm length of the spar is used for  $a$ , and the total 150 mm height of the spar is used for  $b$ , the ratio comes out to 15. This poses a problem, as Figure 3.5 only extends to a ratio value of 6. However, the graphs converge around two values of  $K$ , depending on the clamping assumption.

This leaves the value of  $K_s$  to be in between 5, and 8. The maximum shear bending will occur in the middle of the web. This web, attached to the flanges via the use of stringers, cannot be assumed as clamped, nor can it be assumed as a hinged connection. Nevertheless, for the calculations, values near the clamped assumption are used.

To obtain the locations of valid hole locations, Table 3.5 can be constructed to compare the values of critical buckling shear with and without a hole, with the shear experienced by the spar. According

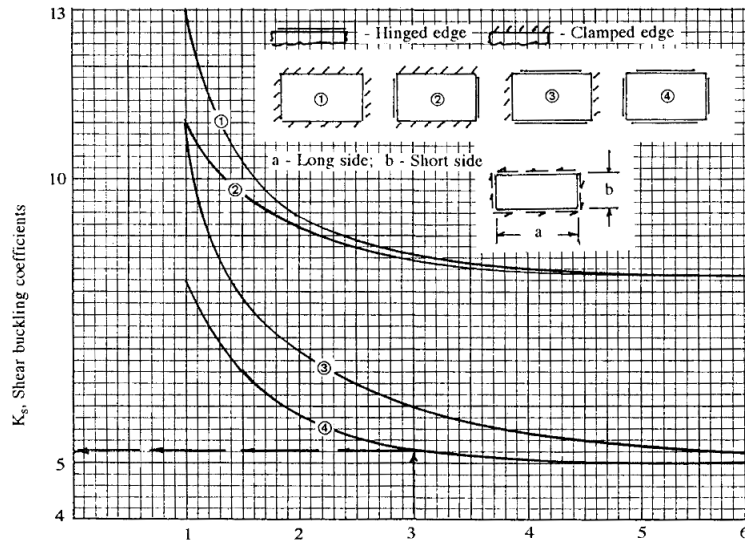


**Figure 3.5:** Shear buckling coefficients for skin-stiffener panel [3]

to [34], the value of the  $K_s$  coefficient in presence of a 40 mm hole surrounded by a 150x150 mm was found to be equal to 66% of the original value and that value was used for calculations.

**Table 3.5:** Buckling Shear Calculations for example values

a/b	$K_s$ continuous	$K_s$ at hole	location [m]	critical shear [MPa]	critical shear at Hole [MPa]	experienced shear [MPa]
1.00	11	7.26	0.15	22.43	14.8	12.78
...	...	...	...	...	...	...
5.00	8.2	5.4	0.75	16.72	11.04	12.98
...	...	...	...	...	...	...
10	8.1	5.34	1.5	16.52	10.90	3.71
...	...	...	...	...	...	...
13	8.1	5.34	1.95	16.52	10.90	3.85
...	...	...	...	...	...	...
15	8.1	5.34	2.25	16.52	10.90	0

Provided with Table 3.5, it is now possible to construct Figure 3.6 that visualises the possible hole locations.

As can be seen in Figure 3.6, the critical shear surpasses the experienced shear stress after 0.8 m from the start of the spar. The kink at the 0.15 m location should be ignored as the actual value of  $K_s$  was approximated. Nevertheless, even with lower  $K_s$  values for less optimistic approximation, it can be seen that holes can be comfortably added after the 0.8 m mark. One must remember that no holes were allowed in the last 250 mm of the spar. This leaves around 1200 mm to place the holes. In iterative design steps, the number of holes was chosen to fit the weight requirements. The holes were placed in a zig-zag pattern to maximise the distance between individual holes. This helps with limiting stress flow concentrations.

### 3.3.3. Explanation and Justification of Design Choices

In the design the shear web contains holes. These holes have the function of weight reduction. The holes are positioned according to Figure 3.6, in a way that they will not be the first failure point in the spar and thus do not impact the maximum load of the spar. The zig-zag pattern was established

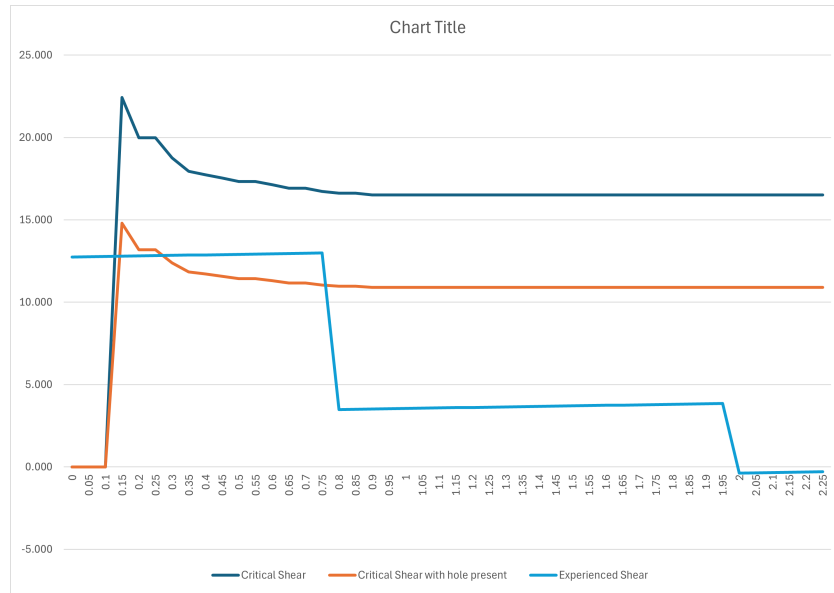


**Figure 3.6:** A shear-location graph comparing critical shear in a continuous sheet (navy blue), critical shear in the presence of a 40mm hole (orange), and the experienced shear stress (blue)

by looking at Figure 3.6 and noting, that a single hole decreased the critical shear by around 30%. Furthermore, the critical shear could be reduced even more until it would become lower than the experienced shear, at which point failure would occur. The zig-zag pattern aimed at maximising the weight reduction, whilst still taking into account the critical shear. As minimizing weight is vital during this project these holes are a strong addition to the design.

To join the spar together the decision was made to use 34 bolts and nuts. This decision came out of the weight requirement, as it is the maximum amount of bolts that can be used while staying under the weight limit of 2552 grams as can be seen in Table 3.6. The reason nuts and bolts were used is for recycling the wing spar. By using nuts and bolts, the parts can be easily disassembled, when it is time to replace the part or retire the aircraft.

**Table 3.6:** Mass calculation of the final beam.

Item	Mass [g]	Amount	Total mass [g]
Sheet X	483.00	1.50	724.50
Sheet Y	128.00	3.00	384.00
L-Stringer Z	237.00	6.00	1422.00
Bolts	1.39	34.00	47.26
Nuts	0.94	34.00	31.96
Holes	2.79	21.00	-58.69
<b>Total:</b>			<b>2551.03 &lt; 2552</b>

The wing spar has to be 2250 mm long. However, the available components from Table 3.1 are all 1500 mm long. It is critical to put thought into how the discontinuities of the parts are positioned. Closer to the root end, the shear stress is greater, thus the web plate has to be continuous to provide maximum strength. The flanges split near the root as they do not provide much resistance against shear. The stringers split in the middle to keep discontinuities far away from each other. The cuts were made with sustainability in mind, in case that, when mass production of the spar commences, the leftover cut parts can be reused.

### 3.4. Final Design

The final design of the spar weighs 2551g and consists of the following elements:

- A full-size X-sheet at the root and a 750mm cut at the tip, both drilled with holes as shown in fig 3.8. These two pieces form the web of the spar.
- Two 750mm Y-sheets at the root and two full-sized ones at the tip, forming the flanges.
- Eight 1125mm stringers, connecting the web to the two flanges.
- 34 bolts and nuts placed as shown in figure 3.7.

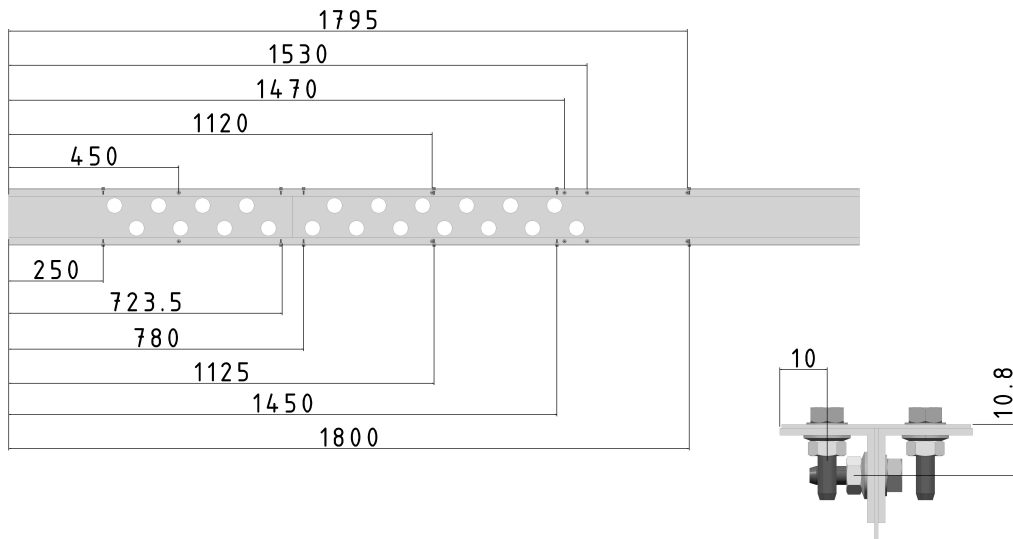


**Figure 3.7: Positioning of the bolts**

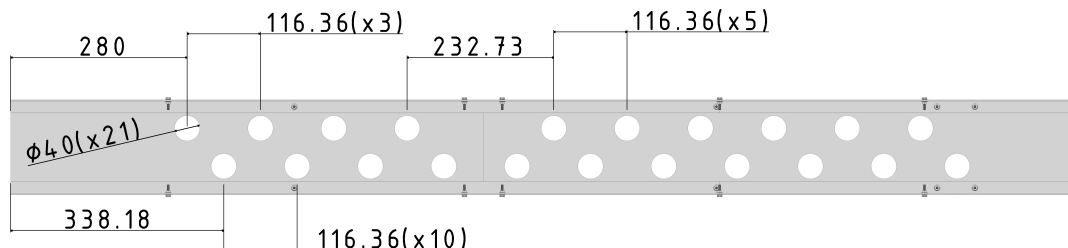


**Figure 3.8: Positioning of the holes**

### Prediction of Failure Load and Mode

There exists an uncertainty of how much drilling a hole lowers the value of the  $K_s$  constant in Equation 3.2. Thus, the team needs to be careful in calculating the amount of lightening holes drilled into the web plate. By being careful with the number of holes, it leaves a limited number of bolts available to meet the mass constraint. Thus, it is expected that the component could fail due to a too little number amount bolts. This would result in buckling in between bolt locations. However, the design team is confident that the buckling will happen above the design constraining applied load of 1.1 kN

Revising the calculations done in Section 3.3 it had been concluded that inter-rivet buckling will be the primary mode of failure for the flanges since this entails the highest amount of uncertainty due to the possibility of non-uniform shear load distribution.

# 4

## Manufacturing of Wing Spar

In this section, the manufacturing plan is discussed. There's an overview of what should be manufactured, how it needs to be made with the necessary dimensions, and an estimation of how much time everything should take. Later in the chapter, there's a reflection, considering how the manufacturing went.

### 4.1. Description of the Manual Production Plan

In this section, the Manual Production Plan will be described. The list of tools and materials can be found in the full, separate production plan and thus only the manufacturing steps are briefly discussed here:

#### 1. Preparation: [15 min]

Put on safety goggles and dress appropriately. Gather all the materials and check if they are in optimal condition.

#### 2. Measuring and Marking: [60 min]

Mark the holes and cuts to be made according to the technical drawings.

#### 3. Layout and Sizing: [40 min]

Now that all the parts are marked it should be checked if the drawn holes align between the parts. The cuts of the sheets and stringers must be made now.

#### 4. Drilling and Lightning Holes: [20 min]

Prepare the plates for drilling. Punch little guides in each marked hole and drill pre-holes. Then the 4 mm drill bit can be used to drill the holes, which should be deburred.

#### 5. Assembly: [10 min]

When all the holes are drilled and finished it is time to start the assembly. Matching the parts exactly to the drawings is crucial to ensure proper fitment. The plates will be attached by running bolts through the holes and securing them with a nut.

#### 6. Final Finishes: [5 min]

Check the finished products to make sure there are no sharp edges, if there are, sand them down. Also, check the tightness of bolts and tighten them when necessary

### 4.2. Assessment of the Predicted vs. Actual Person-hours during Manual Manufacturing

To improve the future predictability of workload, the estimated manufacturing times from the production plan were compared with the actual time spent. To do so accurately, the time spent on each section had been recorded and presented in Table 4.1.

List 4.2 states, explains and justifies the difficulties faced, adjustments made, and deviations from the initial plan during production. Only sections with noticeably large differences are mentioned here.

**Table 4.1:** Comparison of predicted to actual work time per stage

Stage	Predicted [min]	Actual [min]	Difference [min]
Preparation	15	8	-7
Measuring & Marking	60	74	14
Layout & Sizing	40	22	-18
Drilling & Lightening Holes	20	37	17
Assembly	10	11	1
Final Finishes	5	6	1
Total	150	158	8

- **General:** The boundaries between stages were not as harsh as described in the production plan. Since the workforce consisted of five people, parallelising tasks was implemented for efficiency. The hours stated are normalized from the total time each person spent on a given stage divided by the workforce count.
- **Preparation:** This part took less time than expected since all of the materials and most of the tools had already been laid out on the table.
- **Measuring and Marking:** This section took by far the longest and had been underestimated by ~20%. The main reason is, that at most two people could work on drilling the rivet holes, since those require knowledge of the layout and being able to differentiate the stringers from each other to not confuse them.
- **Layout and Sizing:** The process of cutting a metal sheet is easier and faster than had been anticipated and some of the layout work had already been done during the measuring and marking stage.
- **Drilling & Lightening Holes:** Even though, two drills had been provided, only one had been utilized since the drilling activity takes at least two people and occupies a part fully. The task had been parallelized with marking, which occupied the rest of the workforce.

In general, the time estimation was quite accurate in total but was too optimistic and had some major deviations in the individual sections. For future manufacturing sessions, one can expect the total manufacturing time to decrease. Nonetheless, the procedures and stage-duration estimates should be rewritten and refreshed with the observed duration.

### 4.3. Analysis of Nonconformities and Their Influence

During the manufacturing process, mistakes can be made. These result in small deviations, indents, and more: nonconformities. In this section, predictions on nonconformities and their influence on the test outcome will be analysed.

First, there is a chance that a small crack around the hole can occur. It is expected this only has little influence on testing. However, these cracks can propagate over time due to fatigue and load cycles, decreasing the lifetime of the wing.

Second, bolts and rivets may be torqued too loose or too tight. When the bolts are not tight enough, they lose their function. In this case, the spar is more likely to fail in that spot sooner than calculated. It is not expected that not properly tightened bolts will be present in the test sample as it will

be inspected before the test. Over-tightening may damage the bolt/rivet, resulting in potential failure under high stress. Although it is expected that this has little effect on the test results.

Third, any alignment errors while manufacturing may affect the components' strength and integrity. It may lead to e.g. uneven load distributions, stress concentrations and weaker joints. In addition, the acceleration of fatigue damage and crack propagation may compromise the lifetime of the component. If these errors occur it is expected these only have effects long term or when testing failure, not in the prescribed tests.

Last, the product may get damaged during the manufacturing phase, such as by dropping a tool on the component or the component itself. Resulting in small deformations, indents or the bending of a component. These imperfections could impact the final strength of the design depending on the severity of the imperfection, however, in this case, it is assumed to be negligible to the performance of the spar.

Regarding the hypothesis, it is expected that any of the above-listed deviations may happen, because of e.g. machine or human error. These deviations, compared to preliminary calculations and other spars, are not of great influence. But, if tested to failure, loaded cyclic and/or induced fatigue these deviations would noticeably compromise the lifetime of the spar.

#### **4.4. Description of the Robotic Production Plan**

The robotic production plan entails a reasoning for the choice of the KUKA KR210 robotic arm as well as a description of the table and clamp setup, the hole locations and drilling algorithm. The layout for the table setup can be seen in ?? or read about in the robot motion plan.

The drilling of the holes is first being done on the flat panels and then on the 45° angled stringers and routing is done with efficiency and minimal amount of actuation in mind.

#### **4.5. Assessment between Manual and Robotic Manufacturing**

The drilling steps, that is measuring and marking, layout and sizing, and the drilling itself took 5 people approximately 2.5 hours of manual labour. Calculating with the labour cost of 120€/hr per person and 40€/hr for the use of tools and facilities the cost comes up to a total of 1600€.

In case of robotic manufacturing one human supervisor would be enough. It would take an estimated 1 hour to manufacture the spar with 20 minutes of the robot working. Considering this specific production the KUKA KR210 robot would cost an additional 1570€ for the setup, the mould/clamping systems and 370€ for the runtime. The ABB IRB 1200 robot would cost 620€ for the setup and 75€ in terms of runtime. The manual labour for both would be approximately 160€, making the total costs 2100€ for the KUKA KR210 and 850€ for the ABB IRB 1200, as seen in 4.2.

After this initial investment, the robots would only cost their runtime rates. This means for a single spar only the ABB IRB 1200, but for 2 or more spars both types of robotic productions would cost less than manual manufacturing. For mass production, robotic manufacturing does not only save money but time as well. In conclusion, it is practical and cost-efficient in theory, although the training required for the personnel operating the machine and occasional technical problems should also be accounted for.

#### **4.6. Recommendations for Manufacturing**

Robotic manufacturing is chosen for its efficiency. Drilling requires high levels of accuracy and repeatability, performed significantly faster by a robot. For 2 or more spars the cost of manufacturing

**Table 4.2:** Comparison between the cost of robotic and manual manufacturing

	Manual production	KUKA KR210 production	ABB IRB 1200
Manual [hour]	2.5	1	1
People required	5	1	1
Robot [hour]	N.A.	0.33	0.33
Manual labour Cost [€]	1600	160	160
Robot Initial Cost [€]	N.A.	1570	620
Robot Manufacturing Cost[€]	N.A.	363	72.6
Total Cost [€]	1600	2093	852.6

would also be reduced. However, the initial cost for the acquirement of the machinery is significant, making it most feasible for high volumes of production.

# 5

## Sustainability

There is an incentive for IAC to make their design more sustainable. Otherwise, they will lose out on Project Feather Wing to a competitor. This chapter describes the sustainability related to our design.

### 5.1. Economic Model

In most economic sectors a linear model is used which is based on the take-make-use-waste principle. Material is taken from nature and formed into a product. After the product is used it is just thrown away. The linear economy has a lot of disadvantages. No materials are reused which means that sources of materials are being depleted. Besides that waste emits toxic substances which has a negative effect on the environment [35].

To improve their sustainability the IAC should change their economic model from a linear model to a circular model. In a circular model, a used product is being repaired when it does not function anymore and most of the waste is being recycled. This reduces system and material cost and additionally, there will be less emission of greenhouse gasses which will reduce the impact the manufacturing has on global warming.

### 5.2. Manufacturing Waste

During manufacturing of the wing box, a lot of waste is produced because the delivered materials are not exactly the right size for the wing and thus have to be cut to the right length. All the given sheets have a length of 1500 mm as can be seen in table 3.1 and the total wing has to have a length of 2250 mm.

Three web sheets are given, but only two are needed. One sheet will be cut in half and the other will just be attached to its whole length, which means only half a sheet is left. This means the leftover sheet can be used in producing the next spar. For the top and bottom sheets, only three sheets are needed which are all used completely in the design. Eight stringers are provided and all eight stringers are used. They are all cut at a length of 1125 mm. This means that eight stringers with a remaining length of 375 mm are wasted. The Alu-maximum leftover stringers can be used in another part of the aircraft.

### 5.3. Recyclable Aircraft

The tagline of Project Feather Wing is that the new aeroplane has to become a sustainable and 100% recyclable sailplane. This means that every subpart of the aircraft also has to be completely recyclable and thus the recyclability of the wing spar has to be considered. All materials of the wing box should be reused after the end of the life of the wing.

Aluminium plates can be melted and reformed into a new product. The nuts and bolts can be taken out of the wing box. They are made of stainless steel which can also be melted and reformed. This means the total wing box is recyclable.

## 5.4. Explanation and Justification of Design Choices with respect to sustainability

Since sustainability is a major driver for the design of this project, one has to weigh the benefits against the risks of concepts not only in the engineering sense but also with respect to their sustainability. The design choices influenced by sustainability are explained and justified in the list below.

- **Material choice:** Structural design starts with a given material in mind. Since composites are usually designed and manufactured with a given application in mind, they are less versatile than metal structures, which can be manufactured from stock material and reprocessed into different components after their end of service. [36] This makes them less suitable for reuse and thus aluminium had been chosen for its' ease of recycling.
- **Use of stock material:** The most sustainable way of buying aluminium is by doing so in sheets. [37] The process of cutting it into sheets is done very efficiently due to the economy of scale and little to no in-house processing needs to be done to convert raw material into usable parts. This is in stark contrast to other subtractive as well as additive manufacturing techniques, which are way more energy-intensive. [37]
- **Joining method:** When joining parts, one usually takes one of the four options which are bolts, welding, rivets and adhesives. Out of these four, only the bolts allow for easy disassembly without loss of material due to the nature of bolts being screwed in and held in place by shear. For rivets, one would have to drill through the rivet or chip off the heads, which breaks the rivet and wastes material. Adhesives are even worse since there are easy-to-implement and reliable methods for disassembling two parts that are joined by adhesives. Naturally, the decision was made to use bolts.
- **Stronger to avoid cycle fatigue:** To be more sustainable, one can increase the durability of a part and therefore its lifespan. The decision to keep closer to a parts weight requirement in favour of strength opposes the idea of striving for minimum mass but is a calculated step towards prioritizing sustainability and increasing the margin of safety.
- **Cutting locations of stock material:** The raw sheet metal provided comes with specified lengths differing from the lengths needed for the final part. To be as sustainable as possible, one wants to utilize the whole batch of material and keep waste to a minimum. This has been achieved by distributing cuts in a way that optimises the use of the stock material.

## 5.5. Assessment of Spar's Lifetime Cycle

The wing spar is made out of the proprietary aluminium alloy, code-named Alu-maximum. Using this alloy, it must be noted that the extraction and processing of aluminium is not a sustainable process. This part of the life cycle therefore has quite a big impact on the environment.

The Alu-maximum also has to be formed into the right shapes for all the parts that make up the wing spar, which requires energy for the machinery used to do so.

Once the material has been acquired and shaped, the wing spar is manufactured. This was done by hand by the manufacturing department of the IAC, but there is also a possibility of having part of the manufacturing done by a robot. The carbon footprint of this step comes from the energy required by the machinery and the used material. More energy would be needed when using a robot to manufacture the spar, but it would be more efficient.

Afterwards, the wing spar will be integrated in the horizontal stabilizer of the sailplane. Then, once the sailplane has been fully manufactured, it will go to the customer. The customer will then use the sailplane until its lifetime ends. Sailplanes itself do not use engines, which is good for the environment. The system used to get its flight started however is probably not sustainable.

When the sailplane is at its end of life, it will be taken apart. The wing spar will then be taken out and it can be fully disassembled. The Alu-maximum components can be melted and given a new shape for a new purpose, while the bolts can be taken out to be reused. Disassembly and reuse will require energy, but it will make the economy of the wing spar circular, so it is still good for its sustainability.

## 5.6. Explanation and Justification of Manual vs. Robotic Manufacturing

The power consumption for manual manufacturing for 5 people working for 2.5 hours is 1125W. For robotic manufacturing, it is approximately 470W for the KUKA and 920W for ABB with an added 710W each for manual labour. This means the power consumption is less for both robots than the fully manual production. This results in less CO<sub>2</sub> emissions by approximately 0,1kg/spar from the KUKA and 0,2kg/spar from the ABB robot (Table 5.1), if we do not include chain emissions from power stations and production resources.

**Table 5.1:** Comparison of manual and robotic manufacturing energy consumption

	Manual	KUKA KR210	ABB IRB 1200
Total Energy [Wh]	1125	917	710
CO <sub>2</sub> emission with Total Electricity Mix [kg]	0.48	0.39	0.30
CO <sub>2</sub> emission with Grey Electricity Mix [kg]	0.58	0.48	0.37

# 6

## Testing and Analysis

To evaluate the strength and failure characteristics of wing structures, a test setup known as "whiffletree" is used to simulate a distributed load over the length of the wing spar. In the following chapter, the test objectives, setup, instrumentation, and test plan for the previously designed wing spar are described. After a test hypothesis is formed, the test is executed, and then an analysis of the collected data is conducted.

### 6.1. Test Objective and Setup

It is required to test the wing box to see if it meets the requirements set by DELTA. The quantifiable requirements call for a weight of under 2552 grams and that the wing box must not fail while under a load below 1.1 kN. The first requirement is easily checked by weighing the wing box on a gram-accurate scale. The second requirement can be checked by a whiffletree set-up. This setup mimics the distributed load on the wing box during flight. The objective of the tests is to learn if the wing box design is sufficient for the needs of DELTA, and if not to see how the design can be improved.

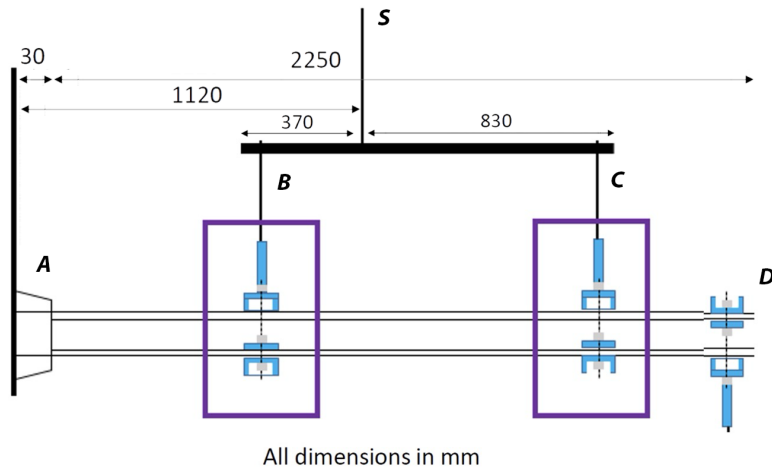


**Figure 6.1:** Side view of whiffletree setup with the load application at Point S.

On the test setup a single load is split into two cables, moreover a weight is hanging at the end, as shown in Figure 6.1. Front and side view of the clamping setup at the two points is shown in Figure 6.2

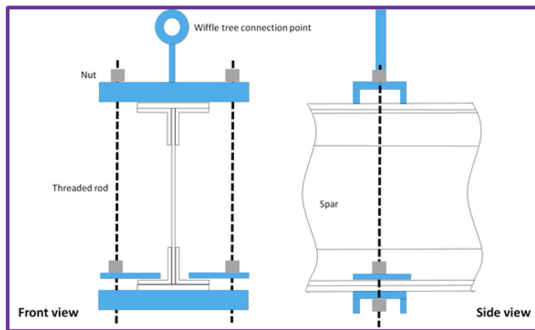


Figure 6.2: Clamp system for whiffletree connection points.

## 6.2. Calculation of load distribution

An equilibrium equation is required to calculate the load distribution over the whiffletree beam. The forces at points B and C from Figure 6.1 must equal the total force on S. The force acting on S equals 1.1 kN according to Section 3.1.

$$\Sigma F_y : 1100 - F_B - F_C = 0 \quad (6.1)$$

To determine the exact value of  $F_B$  and  $F_C$ , a moment equation can be formalized around the pivot point of the beam, S.

$$\Sigma M_S : 0.37F_B - 0.83F_C = 0 \quad (6.2)$$

Combining Equation 6.1 and Equation 6.2 yields the values for  $F_B$  and  $F_C$  which are calculated to be 760.8 N and 339.2 N respectively. The weight of the wing spar can be visualized as a distributed load on the spar. This distributed load  $q$  can be calculated by dividing the spar's mass by its length  $L = 2.25$  m and multiplying it by  $g = 9.81 \frac{\text{m}}{\text{s}^2}$ .

$$q = \frac{F}{L} = \frac{mg}{L} \quad (6.3)$$

This yields a  $q$  of 11.12 N/m. On the end of the wing spar, a weight is suspended. This can be simulated by a point load  $F_D$ . The mass is given to be 5.6 kg which corresponds to a magnitude of 55 N. Knowing all the forces acting on the spar, the reaction forces at the root can be calculated using an equilibrium Equation 6.4 and 6.5 using the directions as can be seen in Figure 6.3.

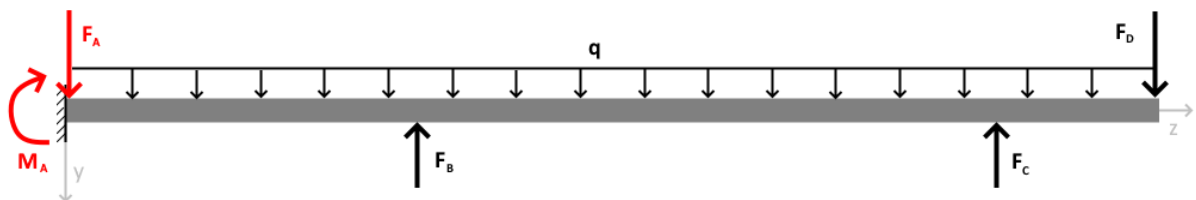


Figure 6.3: Free body diagram of the beam.

$$\Sigma F_y : -F_A + F_B + F_C - F_D - 2.25q = 0 \quad (6.4)$$

$$\Sigma M_A : 0.72F_B + 1.92F_C - 2.25F_D - M_A + 2.25q(1.125) = 0 \quad (6.5)$$

These two equations yield  $F_A$  and  $M_A$  which are calculated to be equal to 1020 N and 1047 Nm respectively. Furthermore, the value of  $F_A$  is at the same time the maximum experienced shear load value. The internal force diagrams that result from these calculations can be found in Figure 3.3.

### 6.3. Utilized Testing Instrumentation

The setup is equipped with two sensors, a load cell Figure 6.4a to measure the total load put on the structure, and a TOF sensor Figure 6.4b to measure its deflection over time.



(a) The location of the Load cell at point S - the main whiffletree cable.



(b) The location of the infrared time of flight sensor, used to measure displacement at the end of the wing spar.

**Figure 6.4: Sensors**

#### Calibration of Sensors:

The TOF sensor is fitted to measure millimetres out of the box, which requires no calibration. This will be confirmed with a measuring tape before testing.

The load cell should be loaded with different weights to get a linear fit from the raw sensor values to the actual weights put on it (Figure 6.5). The mass of the rod must also be taken into account and set to 0 to measure just the contribution of the load system.



**Figure 6.5:** Sensor box test and calibration setup: note the load cell with a rod to add different weights.

## 6.4. Test Plan

Wear safety goggles during the following steps:

1. Prepare the spar:
  - (a) Place the spar with the right side facing up and the right side root positioned correctly in the test machine.
  - (b) Verify the alignment of the spar with the test machine's clamps and supports (Figure 6.1).
2. Drill a hole at the root to fit the clamp:
  - (a) Measure and mark the correct position for the hole at the root of the spar.
  - (b) Remove any debris or burrs from the drilled hole.
3. Install other clamps and set up the weight and rope, following the whiffletree setup diagram (Figure 6.1):
  - (a) Attach additional clamps along the length of the spar as specified by the test requirements.
  - (b) Attach the weight to the end of the beam using the rope.
  - (c) Place restrainers to prevent the weight and rope from slipping off the beam.
4. Check each clamp to ensure it is tightened appropriately.
5. Document the setup:
  - (a) Take pictures of the setup from different angles to document the initial condition.

- (b) Ensure all critical components and configurations are captured in the photographs.
6. Conduct the test:
- (a) Slowly increase the load on the spar while closely monitoring its behaviour.
  - (b) Record a video of the test to capture the progression and any anomalies.
7. Document the failure mode:
- (a) Once the test is concluded, take pictures of the failure mode from different angles.
  - (b) Ensure all aspects of the failure are documented in detail.

## 6.5. Test Events

After the test preparation was complete, each member put on their safety glasses and walked to their station. Three members stood around the setup to film the beam and capture all events, while two others watched all data being plotted by the laptop. In addition, someone turned the handle to increase the load on the beam as the spar was pulled up, and the rest of the team watched the event.

As the spar was pulled up more, it resisted more load. By observation, it was clear the beam started to deflect. This phenomenon lasted until the spar reached a load of  $\pm 1000$  N, at this load the beam started to buckle. Specifically, buckling occurred at the upper part of the web plate and the top sheet close to the clamping, see Figure 6.6.



**Figure 6.6: Buckling at the web plate and top sheet close to the clamp**

The buckling of the web occurred gradually but very little up to  $\pm 1000$  N, in contrast with the buckling of the top sheet. This happened rapidly, as the top sheet suddenly shot up making noise. In addition, during this rapid event the beam deflected 13 mm and a decrease of  $\pm 100$  N was observed. After this event, the load was not increased for a short while to do observations, which can be seen in Figure 6.7 by the small cluster at point (250 mm, 900 N).

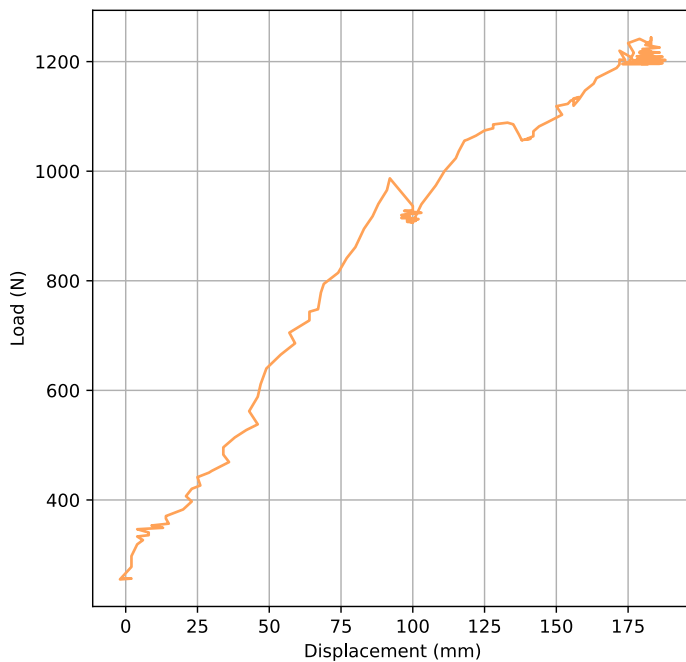


**Figure 6.7:** Plot of the force against displacement during testing. Force vs time and displacement vs time plots are displayed in Appendix A along with the code that generated them.

After the previous event, by observation and the confirmation with Figure 6.7 it was clear that the spar was able to take up more load. The buckling of the top sheet increased and the web plate started to demonstrate severe buckling. Later in time, the spar suffered more serious buckling which can be seen around point (275 mm, 1100 N), resulting in another drop.

This was the last of clear observable events. the load was increased until the testing machine was at its limit. The spar suffered more buckling and deflection, but no event like a snap was observed, by eye or laptop readings. The spar was able to be loaded to  $\pm 800$  N without buckling, and reached a top load of  $\pm 1200$  N when the machine was at its limit. So no failure load was observed.

## 6.6. Failure area analysis

It was clear in the testing that the spar buckled at an applied force of around 1 kN. The buckling occurred right next to where it was clamped to the whiffletree test setup, at the upper portion of the web plate as well as the top sheet. The top flange detached itself from the rest of the spar at this point, as is seen in Figure 6.6.

The problem in the design of the wing spar that caused this might have been that there were no bolts in this area. This part of the wing spar does not have its parts attached well to each other, making the spar weaker in that spot. The spar would have been able to resist forces more effectively had there been bolts present in that location.

Failure load was not measured during the test, since the test setup reached its limit. All that can be said about the limit load of the wing spar is that it is above the experienced 1.2 kN.

## 6.7. Comparison with predictions

The spar was expected to buckle over 1.1kN, but the top sheet ended up buckling at around 1kN. Although the web was continuously buckling it was not critical. The failure occurred between bolts at the top of the spar.

The difference between the test data and the predictions can be explained by underestimating the load the bolts carry, especially at the clamped part of the spar. Another reason for the difference between the test data and the predictions can be that simplifications were made in the calculations that do not capture the complexity of the real world.

It was expected that the primary mode of failure would be inter-rivet buckling. As can be seen in the previous subsection no other form of buckling has occurred and thus this prediction seems quite accurate.

## 6.8. Possible Improvements

The wing spar had performed adequately during the testing, successfully withstanding the loads as required by the IAC. However, there was a rapid deflection around the loading of 1000 N due to the buckling of the web, which ideally must be avoided. Additionally, [some comment about the mass of the spar?]

To tackle the buckling, two things could be done. First, there could have been more reinforcement at the root of the spar to further resist the buckling and second, more rivets could have been used to minimise the buckling of the top flange. Understandably, this would lead to an increase in mass, but there should be a sufficient margin above the specified requirement to ensure success.

If more control was available for the shape of the spar, the wing tips could have been more tapered to reduce the total mass of the spar. It would be feasible as the load experienced by the wingtips is much less than that at the root [33].

# 7

## Conclusion

I claim this task. Will be done during session 11 bartosz

# Bibliography

- [1] Ahmad Alsahlani and Thurai Rahulan, "The Influence of Spar Location on the Elastic Deformation and the Weight Estimation of a Swept-back, High Altitude, Solar Powered Flying Wing UAV," 2017.
- [2] Jelle Wijnja, Roland Schmehl, R. D. B., "Aeroelastic analysis of a large airborne wind turbine," *JOURNAL OF GUIDANCE, CONTROL, AND DYNAMICS*, Vol. 41, No. 11, 8 2018, pp. 2–2.
- [3] Niu, M., *Airframe Stress Analysis and Sizing*, Hong Kong Commilit Press LTD, Hong Kong, 2nd ed., 1999.
- [4] Gudmundsson, S., "Chapter 5 - Aircraft Structural Layout," *General Aviation Aircraft Design (Second Edition)*, edited by S. Gudmundsson, Butterworth-Heinemann, second edition ed., 2022, pp. 113–146.
- [5] "Novel Skin-Reinforcement Design by Cross-Longitudinal Layout Inspired by Dragonfly Wing," .
- [6] "Mechanics of Materials 8th Edition R.C. Hibbeler," .
- [7] Judt, D., Lawson, C., and Lockett, H., "Experimental investigation into aircraft system manual assembly performance under varying structural component orientations," Vol. 234, No. 4, pp. 840–855.
- [8] Eldwaib, K., Grbović, A., and Kastratović, G., "Design of Wing Spar Cross Section for Optimum Fatigue Life," *Procedia Structural Integrity*, Vol. 13, 2018, pp. 444–449.
- [9] Gautam, M., Pandey, B., and Agrawal, M., "Carbon Footprint of Aluminum Production," *Environmental Carbon Footprints*, Elsevier, Amsterdam, 2018, pp. 197–228.
- [10] Grbović, A., Kastratović, G., and Sedmak, A., "Design aspects of light aircraft wing spar—Differential and integral approach," *Material Design & Processing Communications*, Vol. 1, No. 6, 12 2019.
- [11] Cipolla, V., Binante, V., and Nardone, A., "Design, Optimization and Manufacturing of Metallic Wings of Light Aircraft," *Aerotecnica Missili & Spazio*, Vol. 97, No. 4, 10 2018, pp. 219–227.
- [12] Edwards, H. A., Dixon-Hardy, D., and Wadud, Z., "Aircraft cost index and the future of carbon emissions from air travel," *Applied Energy*, Vol. 164, 2 2016, pp. 553–562.
- [13] Sabaghi, M., Cai, Y., and Mascle, C., "Sustainability assessment of dismantling strategies for end-of-life aircraft recycling," *Resources, Conservation and Recycling*, Vol. 102, 9 2015, pp. 163–169.
- [14] Asmatulu, E., Overcash, M., and Twomey, J., "Recycling of Aircraft: State of the Art in 2011," *Journal of Industrial Engineering*, Vol. 2013, 1 2013, pp. 1–8.
- [15] Embry-Riddle Aeronautical University, "Introduction to aerospace flight vehicles - Gliders & Sailplanes," .
- [16] Bachmayer, R., Graver, J., and Leonard, N., "Glider control: a close look into the current glider controller structure and future developments," *Oceans 2003. Celebrating the Past ... Teaming Toward the Future (IEEE Cat. No.03CH37492)*, IEEE, 2003, pp. 951–954.
- [17] Doorn, N. and Ove Hansson, S., "Factors and Margins of Safety," *Handbook of Safety Principles*, edited by M. Niklas, chap. 6, Wiley, 2017, pp. 87–114.

- [18] Clausen, J., Hansson, S. O., and Nilsson, F., "Generalizing the safety factor approach," *Reliability Engineering & System Safety*, Vol. 91, No. 8, 2006, pp. 964–973.
- [19] R. C. Hibbeler, *Mechanics of Materials*, Pearson, 10th ed., 2018.
- [20] Modlin, C. and Zipay, J., "The 1.5 & 1.4 Ultimate Factors of Safety for Aircraft & Spacecraft – History, Definition and Applications," Tech. rep., NASA, 2 2014.
- [21] Beaulieu, A. R., "Margin of Safety Definition and Examples used in Safety Basis Documents and the USQ Process ,," 2013.
- [22] J. A. C. Kentfield, "Structural Loading of Outbound-Horizontal Stabilizer Aircraft Relative to Comparable Conventional Designs," *JOURNAL OF AIRCRAFT*, Vol. 38, No. 1, 2001, pp. 174–180.
- [23] Sullivan, R. W., Hwang, Y., Rais-Rohani, M., and Lacy, T., "Structural analysis and testing of an ultralight unmanned-aerial-vehicle carbon-composite wing," *Journal of aircraft*, Vol. 46, 2009.
- [24] Hendrickson, B. and Devine, K., "Dynamic load balancing in computational mechanics," *Computer Methods in Applied Mechanics and Engineering*, Vol. 184, No. 2-4, 4 2000, pp. 485–500.
- [25] Jansson, N., "Analysis of Dynamic Flight Loads," Tech. rep., Aeronautical and Vehicle Engineering, Stockholm, Sweden, 4 2012.
- [26] Benson, T., "Horizontal Stabilizer - Elevator," *NASA Glenn Learning Technologies Home Page*, 5 2021.
- [27] Shahid, A., Khan, H. A., and Khushbash, S., "Investigation of failure and development of mitigation techniques of a cracked aircraft wing spar cap," *Engineering Failure Analysis*, Vol. 147, 5 2023.
- [28] Carsten Heer, "Robot density rises globally," Tech. rep., International Federation of Robotics, Frankfurt, 2 2018.
- [29] Villani, V., Pini, F., Leali, F., and Secchi, C., "Survey on human–robot collaboration in industrial settings: Safety, intuitive interfaces and applications," *Mechatronics*, Vol. 55, 11 2018, pp. 248–266.
- [30] Golda, G., Kampa, A., and Paprocka, I., "ANALYSIS OF HUMAN OPERATORS AND INDUSTRIAL ROBOTS PERFORMANCE AND RELIABILITY," *Management and Production Engineering Review*, Vol. 9, No. 1, 3 2018, pp. 24–33.
- [31] Satheesh Kumar, K. V., Selvakumar, P., Jagadeeswari, R., Dharmaraj, M., Uvanshankar, K. R., and Yugeswaran, B., "Stress analysis of riveted and bolted joints using analytical and experimental approach," *Materials Today: Proceedings*, Vol. 42, 1 2021, pp. 1091–1099.
- [32] Rośkowicz, M., Godzimirski, J., Jasztal, M., and Gąsior, J., "Improvement of fatigue life of riveted joints in helicopter airframes," *Eksplotacja i Niezawodnosć*, Vol. 23, No. 1, 2021, pp. 165–175.
- [33] "Wing Shapes & Nomenclature," *Introduction to Aerospace Flight Vehicles*, Embry-Riddle Aeronautical University, 2022.
- [34] Abbot Aerospace UK Ltd., "AA-SM-007-004 Effect of Central Hole on Panel Shear Buckling Allowable," 8 2016.

- [35] Sariathli, F., "Linear economy versus circular economy: a comparative and analyzer study for optimization of economy for sustainability," *Visegrad Journal on Bioeconomy and Sustainable Development*, Vol. 6, No. 1, 2017, pp. 31–34.
- [36] Jawaid, M. and Sultan, M. T. H., *Sustainable Composites for Aerospace Applications*, Woodhead Publishing.
- [37] Green, J. A. S., *Aluminum Recycling and Processing for Energy Conservation and Sustainability*, ASM International.

# A

## Plots of Test Data and Events

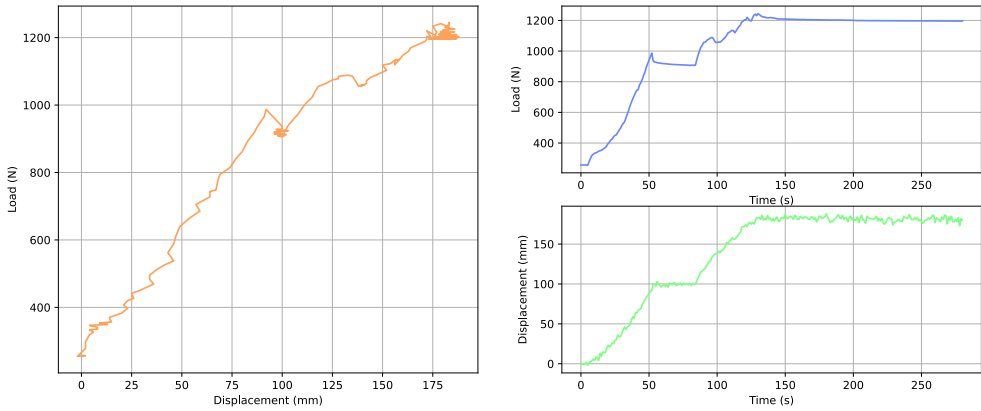


**Figure A.1:** Plots of the collected test data in load vs displacement, load vs time and displacement vs time.

Figure Figure A.1 was generated with the following code:

```
import numpy as np
import matplotlib.pyplot as plt

# Coefficients determined in the test calibration phase
C0_load, C1_load = -49.02, -0.00117
C0_tof, C1_tof = 0, 1

with open('Data_Test_E02G.txt', 'r') as f:
    data = [list(map(float, l.split())) for l in f]

load, displacement = zip(*data)
load, displacement = np.array(load), np.array(displacement) - 150
load = load * C1_load + C0_load

fig = plt.figure(figsize=(15, 6))
fig.canvas.manager.set_window_title('IAC DAQ')
gs1 = fig.add_gridspec(nrows=2, ncols=2) # left=0.05, right=0.48, wspace=0.05
ax1 = fig.add_subplot(gs1[:, 0])
ax2 = fig.add_subplot(gs1[0, 1])
ax3 = fig.add_subplot(gs1[1, 1])

# Plot 1: Displacement vs Load (red color)
ax1.plot(displacement, load, color='#ffa257') # Redish
ax1.set_xlabel('Displacement (mm)')
ax1.set_ylabel('Load (N)')
ax1.grid(True)
```

```
# Plot 2: Time vs Load (blue color)
ax2.plot(range(len(load)), load, color='#6987ff') # Blue in hex
ax2.set_xlabel('Time (s)')
ax2.set_ylabel('Load (N)')
ax2.grid(True)

# Plot 3: Time vs Displacement (green color)
ax3.plot(range(len(load)), displacement, color='#7dff81') # Greenish
ax3.set_xlabel('Time (s)')
ax3.set_ylabel('Displacement (mm)')
ax3.grid(True)

plt.savefig('spar_test.svg', format='svg')
plt.show()
```

*TODO: additional pictures from testing*

# B

## Calculations Done for Beam Hole Placements

a/b	K continous	K at hole	location along beam	critical shear MPa	critical shear hole	Shear Force N	experienced shear MPa
0.00		0	0	0.000	0.000	1020.056	12.75070237
0.33		0	0.05	0.000	0.000	1021.308	12.76634397
0.67		0	0.1	0.000	0.000	1022.559	12.78198558
1.00	11	7.26	0.15	22.434	14.807	1023.810	12.79762719
1.33	9.8	6.468	0.2	19.987	13.191	1025.062	12.81326879
1.67	9.8	6.468	0.25	19.987	13.191	1026.313	12.8289104
2.00	9.2	6.072	0.3	18.763	12.384	1027.564	12.84455201
2.33	8.8	5.808	0.35	17.947	11.845	1028.815	12.86019361
2.67	8.7	5.742	0.4	17.743	11.711	1030.067	12.87583522
3.00	8.6	5.676	0.45	17.539	11.576	1031.318	12.89147683
3.33	8.5	5.61	0.5	17.335	11.441	1032.569	12.90711843
3.67	8.5	5.61	0.55	17.335	11.441	1033.821	12.92276004
4.00	8.4	5.544	0.6	17.132	11.307	1035.072	12.93840165
4.33	8.3	5.478	0.65	16.928	11.172	1036.323	12.95404325
4.67	8.3	5.478	0.7	16.928	11.172	1037.575	12.96968486
5.00	8.2	5.412	0.75	16.724	11.038	1038.826	12.98532647
5.33	8.15	5.379	0.8	16.622	10.970	279.244	3.490551406
5.67	8.15	5.379	0.85	16.622	10.970	280.495	3.506193013
6.00	8.1	5.346	0.9	16.520	10.903	281.747	3.52183462
6.33	8.1	5.346	0.95	16.520	10.903	282.998	3.537476227
6.67	8.1	5.346	1	16.520	10.903	284.249	3.553117833
7.00	8.1	5.346	1.05	16.520	10.903	285.501	3.56875944
7.33	8.1	5.346	1.1	16.520	10.903	286.752	3.584401047
7.67	8.1	5.346	1.15	16.520	10.903	288.003	3.600042654
8.00	8.1	5.346	1.2	16.520	10.903	289.255	3.61568426
8.33	8.1	5.346	1.25	16.520	10.903	290.506	3.631325867
8.67	8.1	5.346	1.3	16.520	10.903	291.757	3.646967474
9.00	8.1	5.346	1.35	16.520	10.903	293.009	3.662609081
9.33	8.1	5.346	1.4	16.520	10.903	294.260	3.678250687
9.67	8.1	5.346	1.45	16.520	10.903	295.511	3.693892294
10.00	8.1	5.346	1.5	16.520	10.903	296.763	3.709533901
10.33	8.1	5.346	1.55	16.520	10.903	298.014	3.725175508
10.67	8.1	5.346	1.6	16.520	10.903	299.265	3.740817114
11.00	8.1	5.346	1.65	16.520	10.903	300.517	3.756458721
11.33	8.1	5.346	1.7	16.520	10.903	301.768	3.772100328
11.67	8.1	5.346	1.75	16.520	10.903	303.019	3.787741935
12.00	8.1	5.346	1.8	16.520	10.903	304.271	3.803383541
12.33	8.1	5.346	1.85	16.520	10.903	305.522	3.819025148
12.67	8.1	5.346	1.9	16.520	10.903	306.773	3.834666755
13.00	8.1	5.346	1.95	16.520	10.903	308.025	3.850308362
13.33	8.1	5.346	2	16.520	10.903	-29.891	-0.373633365
13.67	8.1	5.346	2.05	16.520	10.903	-28.639	-0.357991758
14.00	8.1	5.346	2.1	16.520	10.903	-27.388	-0.342350151
14.33	8.1	5.346	2.15	16.520	10.903	-26.137	-0.326708545
14.67	8.1	5.346	2.2	16.520	10.903	-24.885	-0.311066938
15.00	8.1	5.346	2.25	16.520	10.903	-23.634	-0.295425331

# C

## Statement on AI Usage

**Table C.1:** *AI tools Used*

<b>Tool</b>	<b>Chapter</b>	<b>Use</b>
Grammarly	-	Spelling, punctuation, and grammar checking.
ChatGPT	Literature Study	Give a short summary and entry point for continuing specific topic search
Consensus		

D

## Gantt Chart

*finalGanttchart*

# E

## Task Distribution

*taskdistribution*